DESIGN AND FABRICATION OF PZT-ACTUATED SILICON SUSPENSIONS

Tsung-Lin (Tony) Chen and Roberto Horowitz

December 11, 2000

A silicon suspension, suitable for use in a piezoelectrically actuated dual-stage servo system for magnetic Hard Disk Drives (HDDs), has been designed, fabricated and partially tested. The suspension has an integrated gimbal structure and features that are useful for attaching PZT ($Pb(Zr_xTi_{1-x})O_3$) strips. Under a 15 V applied voltage, the PZT strips stretch the suspension, producing an effective 0.5 μm magnetic head radial motion. The suspension has an in-situ piezoresistive film, which produces a signal proportional to the in-plane suspension bending. This signal can be used as an additional relative position error signal, which greatly improves the robustness of the track-following HDD servo. Microfabrication techniques, suitable for fabricating this high performance one-piece silicon suspension, are also presented.

1 INTRODUCTION

The areal data density of magnetic Hard Disk Drives (HDDs) is increasing at the annual rate of more than 60%. Products available on market have a storage areal density that is close to 10 Gbit/in^2, and will soon have storage densities approaching 35 Gbit/in^2. It is well known that two of the main factors that limit further performance improvements are the friction and other nonlinearities present in the voice coil motor (VCM) ball bearings and the existence of multiple structural resonance modes in the VCM, E-block and suspension. It has been proposed that one possible solution to overcome these limitations is to incorporate a secondary actuator, which moves the magnetic head relative to the suspension, and implement a dual-stage servo [3] [1] [13] [11] [6]. This secondary actuator has to be capable of extending the dual-stage bandwidth beyond 2 KHz, in order to provide enough low

frequency attenuation of friction and windage disturbances and to counteract suspension vibration induced runout.

There are many papers in the literature that report on the design and implementation of piezoelectrically actuated suspensions as a means of dual-stage actuation (see for examples [5] [2]). In most designs, the piezoelectric actuators are placed between the E-block and the suspension, to produce a sufficiently large magnetic head motion. This arrangement is effective in designing dual-stage servo system that attain large low frequency runout attenuation, but may be susceptible to instabilities due to the excitation of suspension resonance modes.

Most dual-stage servo controllers only utilize the position error signal (PES) of the magnetic head relative to the center of data track for closed-loop track following control. These systems have a single-input-multi-output (SIMO) control architecture. However, in some instances, it is also possible to measure the relative position error signal (RPES) of the magnetic head relative to the VCM. In this case, the control architecture is multi-input-multi-output (MIMO). As shown in [6], the RPES can be used in a MIMO controller to damp out the second stage actuator's resonance mode and enhance the overall robustness of the system.

In this report, we propose a new suspension design, which allows the placement of piezoelectric (PZT) actuators on the suspension, at a location that is very closed to the gimbal, while still achieving a 0.5 μm of magnetic head radial motion. Thus, in this configuration, the secondary actuators not only are able to attenuate low frequency runout, but also are able to partially compensate for runout induced by E-block and suspension vibration. Moreover, the design incorporates in-situ piezoresistor films, which produce a signal proportional to the deflection of the suspension when it is flexed by the PZT actuators, and can be used as the RPES in a MIMO dual-stage servo control architecture.

The field of micro-electromechanical systems (MEMS) is growing rapidly. Micromechanical structures are currently being investigated for a wide variety of applications because they are generally several orders of magnitude smaller than their conventional counterparts, can easily be integrated with electronic circuits and can potentially achieve high performance with low fabrication costs. The use of silicon as the MEMS structure material has been summarized by [9]. Current deep reactive ion etch (DRIE) processes

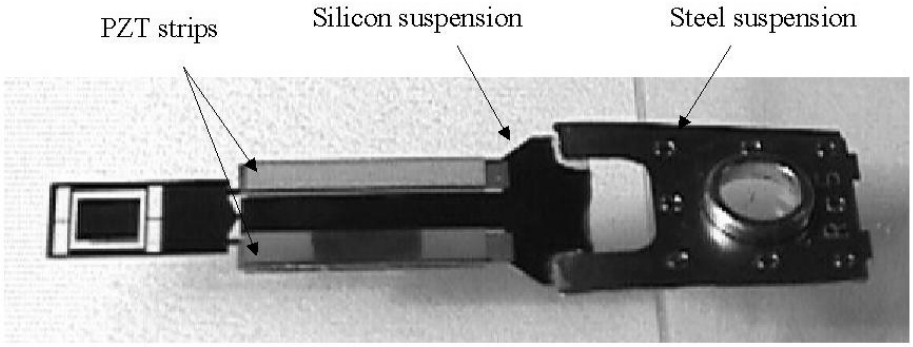

Figure 1: Prototype of PZT-actuated silicon suspension

are able to achieve high aspect ratio (> 25:1) mechanical structures and make the micromachining a more promising fabrication technique for actuators as well as sensors [4]. This report also presents a microfabrication process for building a proposed one-pieced silicon suspension design, which is suitable for PZT actuation, and has an integrated gimbal, an in-situ RPES sensor and electrical interconnects.

2 DESIGN OF PZT-ACTUATED SILICON SUSPENSIONS

Fig. 1 shows a photograph of our PZT-actuated silicon suspension prototype. The suspension was micro-fabricated using single-crystal silicon as the structure material and has an in-situ piezoresistive film (piezoresistor) deposited on it. Four pieces of bulk PZT strips must be glued to the silicon suspension: one pair is glued on top side, the other on the bottom. These PZT strips leverage in a push-pull scheme and move the magnetic head in the in-plane radial direction. When the PZT stretches the suspension to position the magnetic head, it also stretches the deposited piezoresistive film. This piezoresistor produces an electrical signal that is proportional to its deformation and can be used to determine the position of the magnetic head relative to the VCM, this signal is known as the RPES. The silicon suspension is subsequently glued to a pre-cut steel portion, as shown in the figure. This pre-cut steel suspension is pre-bent and has a pivot which is attached to the E-block. The pre-bend in the steel portion of the suspen-

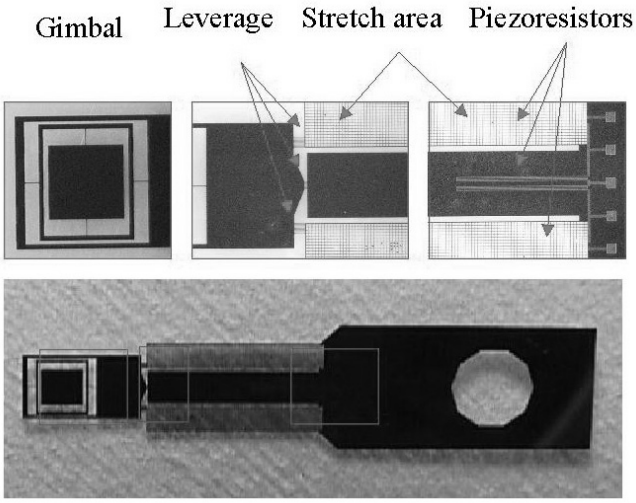

Figure 2: Features on silicon suspension

sion is necessary to provide a downward pre-load force on the slider, which counteracts the air bearing forces that act on the slider when it flies on top of the rotating hard disk. The steel-silicon suspension assembly shown in Fig. 1 has the same boss-to-gimbal length as most commercial products.

2.1 Silicon suspension

The silicon suspension designed incorporates several special features for enabling PZT actuation. These enhance the dual-stage PZT actuation performance and lower the required driving voltage. The design also features an integrated gimbal structure, which can lower assembling efforts and fabrication costs to a great extend. These features are shown in the Fig. 2 and are discussed below:

Stretch area: This is the area where the PZT strips are attached. Deep trenches that cut all the way through the suspension delimit it. Inside this area, it consists of very sparse grids, as it is shown in Fig. . Thus equivalent Young's modulus of this area is less than the remaining sections of the silicon suspension [7]. This area was designed to lower the driving voltage on the PZT strips, while the overall suspension can still be sufficiently stiff to meet other performance requirements.

Leverage structure: The leverage structure transforms the axial push-pull movement of the PZT strips into an in-plane angular motion of the integrated gimbal structure. This structure was designed to be soft in in-plane bending but stiff in out-of-plane bending. This decreases the PZT actuation force required to rotate the gimbal, while transmitting the necessary vertical pre-load force to the picoslider. To achieve this goal, the leverage structure was designed to consist of 3 sets of high aspect flexures, instead of 3 planks. Each flexure is 10 mm wide and 80 mm high. There are two main reasons for selecting flexures instead of planks. 1) A simple calculation shows that, given an aspect ratio of 8, the in-plane bending vs. out-of-plane bending stiffness ratio is 1:82. Moreover, using 3 sets of flexures instead of 3 planks reduces the in-plane bending stiffness by roughly 81 folds, while preserving the same amount of out-of-plane bending stiffness. 2) A finite Element simulation (FEM) indicates that this leverage structure is subjected to the highest level of stress of the entire suspension. Researches have shown that the fracture strength for single crystal silicon depends on the dimension of the cross-section. According to [10], "the smaller the cross-section, the higher the strength." Lastly, the proposed leverage structure design amplifies by a factor of three the PZT stretch motion, as it is transmitted to magnetic head.

RPES sensors: An in-situ piezoresistor pattern was deposited both in the stretch areas and in the center area of the suspension, which does not stretch, to form a Wheatstone resistor bridge. This resistor bridge produces a voltage signal that is proportional to the amount of stretch produced by the PZT strips, while reducing the effect of resistance variations in the piezoresistive material due to temperature.

Gimbal structure: The most challenging part of the integrated gimbal structure design is to design the torsion bars, which produce the necessary pitch and roll gimbal flexibility, while providing as high as possible in-plane bending stiffness. In order to keep the fabrication process of the overall suspension as simple as possible, all elements of the gimbal structure, including the torsion bars, were designed to have the same thickness as the rest of suspension. Moreover, in order to leave sufficient space for running the necessary wires through the torsion bars of the suspension, the minimum width of the torsion bars was pre-determined. Given the limited choices of parameter variations, the design has to match all gimbal and suspension dynamics requirements. In this report, we present two different gimbal designs, as shown in Fig. 3. Design I uses one flexure on each side of the gimbal structure as

the torsion bar; while Design II has two adjacent flexures. The dimensions for these two designs are listed in the Table 1. More design flexibility can be achieved if the fabrication process is designed so that the thickness of the torsion bars is smaller than the rest of the structure and a face sheet is laid on top of the torsion bars for cable wiring [8].

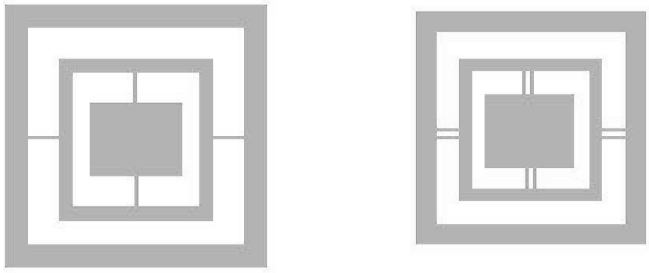

Figure 3: Two silicon gimbal designs

Unit:μm	Design I (1 flexure)	Design II (2 flexures)
Roll flexures	230*16*80	150*10*80
Pitch flexures	250*16*80	170*10*80

Table 1: Dimensions of gimbal torsion bar

2.2 FEM simulation

Table 2 shows the FEM simulation results of the two silicon gimbal designs proposed in this paper, and compares these designs with a commercial product (the TSA series, produced by Hutchinson Technology Inc.) and a silicon gimbal design proposed by [12]. Design II has higher in-plane bending stiffness as compared to the Design I. Moreover, it also has more space to run wires through the torsion bars. However, Design II is not feasible unless the trench etch aspect ratio is increased to twenty. Both designs have the compatible performance with TSA series. However, Design I and II are one-piece suspensions, while the TSA series are 2-piece suspensions (Load beam and Flexure). The silicon gimbal design in [12] has serpentine microsprings as the torsion bars, and its roll and pitch stiffness do not fall in the range of the TSA series.

Table 3 shows the silicon suspension (Design I) FEM performance predictions and compares them with a commercial TSA2030 steel suspension.

	Design(I)	Design (II)	TSA series	Silicon gimbal (Wu)
Roll (μNm/deg)	1.14	1.4	0.85–1.5	1.9
Pitch (μNm/deg)	1.07	1.16	0.85–1.5	2.5
Sway (KHz)	9.4	11.3	6.8–10.5	9.7
Out-of-plane stiffness(KN/m)	8.24	11.5		0.198

Table 2: FEM of silicon gimbal design

All steel, silicon, PZT, epoxy components of the suspension structure are modeled in the simulation, as well as the picoslider. According to the FEM results, the first torsional mode of the suspension is due to the steel component, which is located between the PZT strips and the E-block pivot point (see Fig. 1). This resonant mode is about 2.6 kHz and will probably be the first resonance encountered by the VCM section of the dual-stage servo. The 2nd torsion mode is about 7.8 kHz and is due to the two stretch areas moving up and down. The push-pull actuation scheme in this suspension design produces a small asymmetry along the out-of-plane direction, which can excite this resonant mode. Therefore, this mode is predicted to be the first resonance mode that will be encountered by the second-stage PZT component of the dual-stage servo, and may limit the overall bandwidth of the system.

	New Design	TSA2030
1st Bend	20 N/m	14.7 N/m
2nd Bend	2621 Hz	1640 Hz
1st Torsion	2645 Hz	2720 Hz
2nd Torsion	7781 Hz	6500 Hz
3rd Bend	4755 Hz	
1st Sway	9908 Hz	10900 Hz

Table 3: FEM results of steel–silicon suspension

The FEM simulations also predict that the magnetic head can move 1 μm statically, when 20 Volts are applied to the PZT strips. At this level of stretch, the maximum stress is about 0.5 Gpa, assuming that a 2 gram vertical load is acting on the picoslider. The fracture strength for microma-

chining single crystal silicon is reported to be between 2–7 GPa [10].

3 FABRICATION PROCESS

A simple and reliable SOI-like fabrication process has been developed for fabricating these structures. This process is compatible with most surface micromachining processes. However, it offers the advantage that it produces high aspect ratio 3-dimensional structures without requiring costly SOI wafers. The starting material is a highly conductive, double sides polished, 1-0-0 wafer. The process uses an Inductive Coupled Plasma (ICP) system to pattern high aspect ratio silicon structures. The structures and trenches are subsequently coated with a thin layer of silicon nitride, for protection from KOH etcher attack. The structures are released by the KOH backside etch. Lastly, a timed HF etch strips the silicon nitride protection layer from the structure. The fabrication process flow is shown in the Fig. 4.

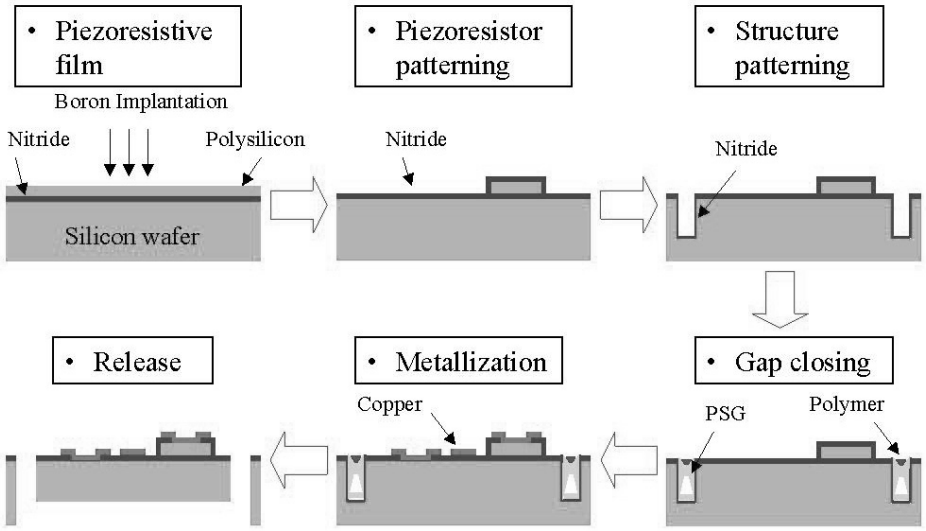

Figure 4: Silicon suspension fabrication process flow

4 RESULTS AND DISCUSSION

Fig. 5 shows a schematic drawing of the experimental setup. A laser Doppler Velocimeter (LDV) is aimed at the end of the PZT stretch area, to measure

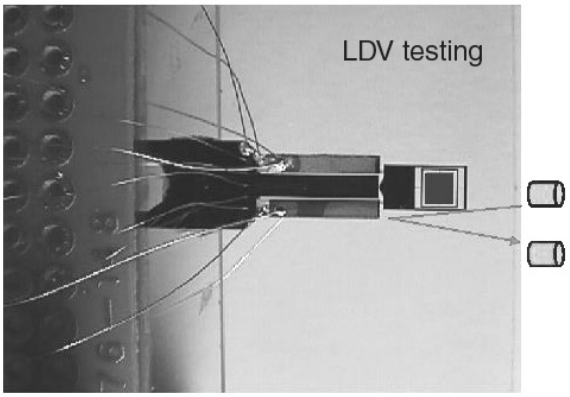

Figure 5: PZT actuation testing

its motion.

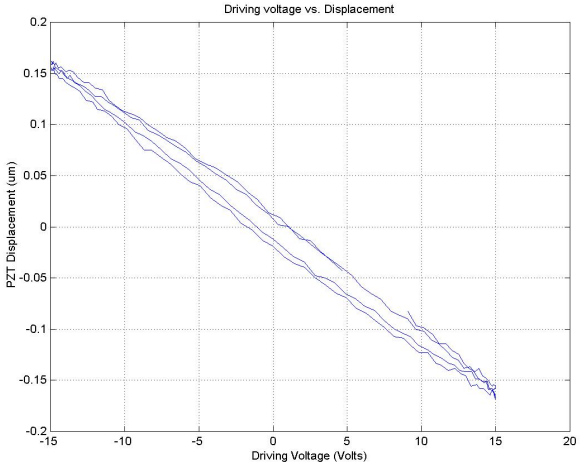

Figure 6: Characteristics of PZT actuators, input voltage at 1 KHz

Fig. 6 and Fig. 7 show that the PZT actuators can move +/- 0.16 μm under a 1 KHz input excitation with a 15 Volt amplitude. With the magnitude amplification of 3 from the leverage structure, this motion results in a +/- 0.5 μm magnetic head motion along the radial direction. The first structural resonant mode is observed to be at about 7 KHz which agrees with the 2nd torsion mode of FEM simulation as shown in Table 3. Although this experiment is done without picoslider attached to the gimbal structure, it is

predicted that the resonant mode for PZT actuation would still be around 7 KHz with picoslider on it due to the light weight of picoslider comparing with PZT strips. The first torsion mode doesn't show up in this experiment because the suspension is not fixed at pivot point, see Fig. 5. From Fig. 6, a phase lag between driving voltage and PZT displacement has been observed but not hysteresis effect. The lines are not coincident in Fig. 6 and it is due to the drift in LDV setup.

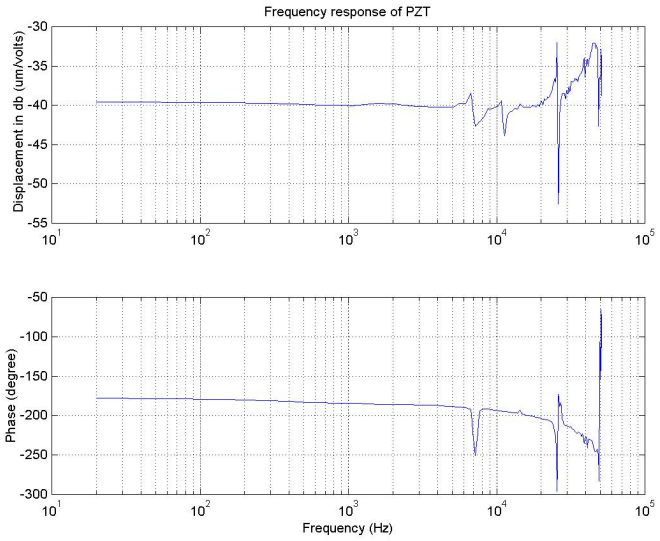

Figure 7: Frequency response of PZT actuators. The resonant frequency is 7 KHz w/o the picoslider

The characterization of the RPES sensors was preceded by applying an input voltage to the PZT actuators and measuring the output of the piezoresistive Wheatstone Bridge. The experimental data in Fig. 8 shows a linear response of the piezoresistor bridge. The sensitivity of this piezoresistive film is calculated to be 1.81 KΩ/ μm. It corresponds to the gauge factor of 30. The output of the Wheatstone resistor bridge is 12.13 mv/ μm under 5 V dc bias. A large feedthrough was observed during the experiment from the input voltage applied to the PZT actuators to the piezoresistors RPES output. To better understand this problem, a simple resistance-capacitance circuit model was derived, as shown in Fig. 9.

It suggests that the feedthrough is due to the finite resistance of the epoxy used to glue the PZT strips to the silicon suspension in the stretch

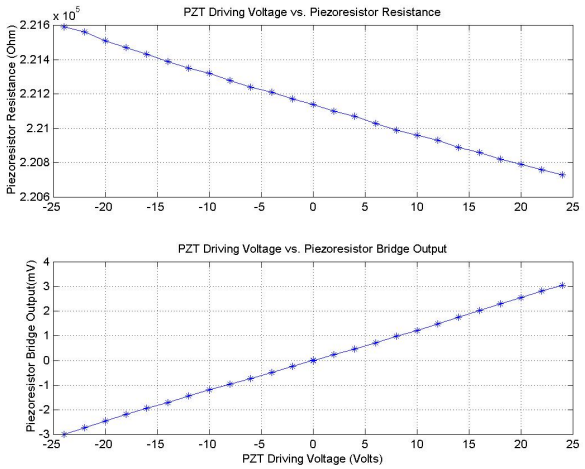

Figure 8: Characteristics of Piezoresistors

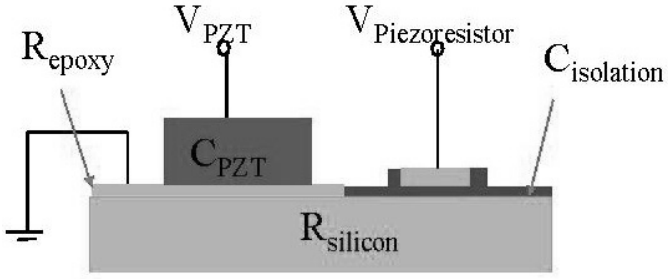

Figure 9: A resistor-capacitor schematic drawing for PZT actuated silicon suspension

areas. Unfortunately, the driving voltage for PZT actuators has a magnitude in the tens of Volts, while the position-sensing signal produced by piezoresistor bridge is at the mini-volt level. Thus, the resistance of epoxy would have to be in the milli-ohm level, in order to meet the SNR (signal-noise-ratio) specification for RPES. This suggests that using a more conductive epoxy than the one used to assemble the prototype will not solve this problem completely. Another solution to the feedthrough problem is to use a frequency modulation technique in this piezoresistors bridge. A simple frequency modulation scheme was successfully implemented and the results are shown in Fig. 10.

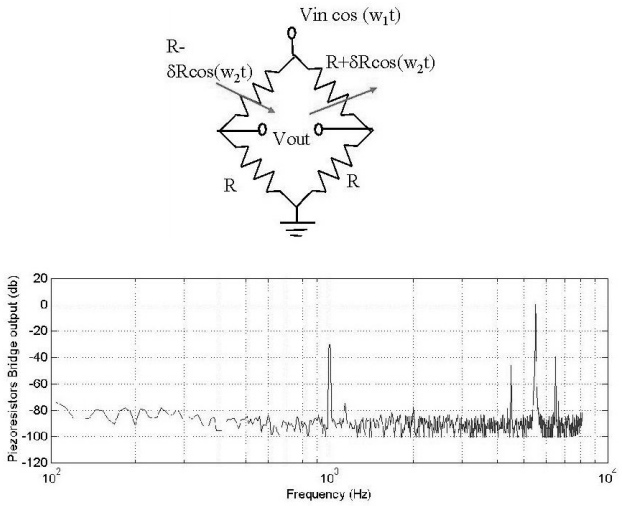

Figure 10: Modulation for the piezoresistors sensing bridge

5 CONCLUSION

A one-piece silicon suspension was designed, fabricated and tested, which can be flexed by piezoelectric PZT strips and used as a second-stage actuator in a dual-stage servo system. The PZT actuation is able to drive the magnetic head +/- 0.5 μm with +/- 15 Volts applied on the PZT strips, without any obvious hysteresis effect. The suspension also has an integrated gimbal structure. The first resonance mode frequency of this structure is about 7 KHz. The performance of the suspension is predicted by FEM simulation to be similar to that of commercially available steel suspensions. The im-

plemented piezoresistors RPES sensing scheme has a fairly linear response and a high sensitivity (Gauge Factor). A large feedthrough from driving signal to sensing signal has been observed. It was attributed to the small electrical resistance of the conductive epoxy that was used to glue the PZT strips to the silicon structure. The use of a higher conductivity epoxy will not significantly alleviate this problem, due to the 80 dB magnitude difference between the driving and sensing signals. An alternative solution to the feedthrough problem is to apply a frequency modulation technique to the sensing scheme. The feasibility of frequency modulation was demonstrated by the experimental data.

References

[1] Cheung, P., Horowitz, R. and Howe, R. (1996). Design, Fabrication, Position Sensing and Control of an Electrostatically-driven Polysilicon Microactuator. *IEEE Transactions on Magnetics*,**Vol. 32, No. 1**, pp 122–128.

[2] Evans, R. B., Griesbach, J. S. and Messner, W. C. (1999). Piezoelectric Microactuator for Dual Stage Control. *IEEE Trans. on Magnetics*, **Vol. 35 No. 2**, pp 977–982.

[3] Fan, L. S., Ottesen, H. H., Reiley, T. C. and Wood, R. W. (1995). Magnetic Recording Head Positioning at Very High Track Densities Using a Microactuator-based Two-stage Servo System. *IEEE Trans. on Industrial Electronics*, **Vol, 42, No. 3**, pp 222–233.

[4] Kuhl, Karl, Vogel, Stefan Schaber, Ulrich, Schafflik, Rainer and Hillerich, Bernd (1998). Advanced Silicon Trench Etching in MEMS Applications. *SPIE Conference on Micromachining and Microfabrication Process*. **Vol. 3511**, pp 97–105.

[5] Mori, K., Munemoto, T., Otsuki, H., Yamaguchi, Y., Akagi, K. (1991). A Dual-Stage Magnetic Disk Drive Actuator Using a Piezoelectric Device for a High Track Density. *IEEE Trans. on Magnetics*. **Vol. 27, No. 6**, pp 5298–5300.

[6] Li, Y. and Horowitz, R. (2000). Track-Following Controller Design of MEMS Based Dual-Stage Servos in Magnetic Hard Disk Drives. *International Conference on Robotics and Automations*. April, 2000. San Francisco, USA.

[7] Lorna J., Gibson (1988). Cellular Solids. pp 114–115. Oxford, New York: Pergamon Press.

[8] Muller, L., Heck, J. M., Howe, R. T. and Pisano, A. P. (2000). Electrical Isolation Process For Molded, High Aspect Ratio Polysilicon Microstructures. *Proceedings of IEEE Workshop on Micro Electro Mechanical Systems (MEMS2000)*, pp 590–595.

[9] Peterson, Kurt E. (1982). Silicon as a Mechanical Material. *Proceedings of the IEEE*, **Vol. 70, No. 5**, pp 420–457.

[10] Peason, G. L., Read, W. T. and Feldmann, W. L. (1957). Deformation and Fracture of Small Silion Crystals. *ACTA METALLURGICA*, **Vol. 5**, April, pp 181–191.

[11] Roberto Oboe, A. B. and Murari, B. (1999). Modelling and Control of a dual stage actuator hard disk drive with piezoelectric secondary actuator. *International Conference on Advanced Intelligent Mechatronics*, September, Atlanta, USA, pp 138–143.

[12] Wu, Shuyun, Temesvary, Viktoria, Tai, Yu-Chong and Miu, D. K. (1996). Silicon micromachined integrated suspension systems for magnetic disk drives. *Sensors and Actuators*, **A55**, pp 195–200.

[13] Takaishi, K., Imamura, T. Mizoshita, Y., Hasegawa, S., Ueno, T. and Yamada, T. (1996). Microactuator Control For Disk Drive. *IEEE Transaction on Magnetics*, **Vol. 32, No. 3**, pp 1863–1866.